

ARCHIVAL REPORT

Transcriptome Analysis of the Human Striatum in Tourette Syndrome

Jessica B. Lenington, Gianfilippo Coppola, Yuko Kataoka-Sasaki, Thomas V. Fernandez, Dean Palejev, Yifan Li, Anita Huttner, Mihovil Pletikos, Nenad Sestan, James F. Leckman, and Flora M. Vaccarino

Background: Genome-wide association studies have not revealed any risk-conferring common genetic variants in Tourette syndrome (TS), requiring the adoption of alternative approaches to investigate the pathophysiology of this disorder.

Methods: We obtained the basal ganglia transcriptome by RNA sequencing in the caudate and putamen of nine TS and nine matched normal control subjects.

Results: We found 309 downregulated and 822 upregulated genes in the caudate and putamen (striatum) of TS individuals. Using data-driven gene network analysis, we identified 17 gene co-expression modules associated with TS. The top-scoring downregulated module in TS was enriched in striatal interneuron transcripts, which was confirmed by decreased numbers of cholinergic and gamma-aminobutyric acidergic interneurons by immunohistochemistry in the same regions. The top-scoring upregulated module was enriched in immune-related genes, consistent with activation of microglia in patients' striatum. Genes implicated by copy number variants in TS were enriched in the interneuron module, as well as in a protocadherin module. Module clustering revealed that the interneuron module was correlated with a neuronal metabolism module.

Conclusions: Convergence of differential expression, network analyses, and module clustering, together with copy number variants implicated in TS, strongly implicates disrupted interneuron signaling in the pathophysiology of severe TS and suggests that metabolic alterations may be linked to their death or dysfunction.

Key Words: Basal ganglia, immune system, interneuron, network, nitric oxide synthase (NOS), RNA-Seq

Tourette syndrome (TS) is a childhood-onset neuropsychiatric disorder characterized by motor and vocal tics with a population prevalence estimated to be 1% to 3% and frequent comorbidity with obsessive-compulsive disorder and attention-deficit/hyperactivity disorder (1). Twin studies suggest a substantial genetic contribution (2), but genome-wide association studies have not revealed any risk-conferring common genetic variants (3,4). Rare mutations have been identified in two genes (*SLITRK1* and *HDC*), but it remains unclear whether and to what degree these mutations provide insights applicable to the majority of TS cases (5,6). Environmental factors and autoimmunity have been also implicated in TS pathogenesis, as maternal smoking (7), low birth weight (8), familial autoimmune disease, and immune dysfunction (9,10) are more prevalent in TS patients. In a small proportion of cases, this disorder is associated with an infectious event and accompanied by immunoreactive changes in the peripheral blood (9).

Changes in volume of several brain regions have been reported in TS (11–15); however, disruptions in corticostriatal

circuitry have most consistently been implicated in this disorder [for reviews, see (16,17)]. Structural neuroimaging studies revealed a 5% reduction in caudate volume in TS (12) and suggested that smaller caudate volumes in childhood are significantly correlated with persistent symptom severity in adulthood (15). Postmortem analyses of brain tissue from patients with lifelong TS demonstrated reductions in immunohistochemical markers for cholinergic and parvalbumin⁺-gamma-aminobutyric acid (GABA)ergic interneurons in the caudate and putamen (18,19). However, whether interneurons are lost or whether the cells simply downregulate protein marker expression due to some other unrelated mechanism is unknown.

To analyze the neurobiology of TS in an unbiased fashion, we characterized the transcriptome of the caudate and putamen of nine TS individuals with documented unremitted symptoms compared with nine matched normal control (NC) subjects. Differential gene expression and unbiased, data-driven gene co-expression network analyses allowed us to identify genes and gene networks that distinguish brain tissue of individuals with chronic TS from that of unaffected individuals. Our findings provide the first direct evidence for two separate neurobiological factors playing a role in the disorder, decreased signaling of multiple classes of striatal interneurons and dysregulated activation of the immune system.

Methods and Materials

Subjects

TS brain samples of cases with refractory symptoms in adulthood, collected by the Tourette Syndrome Association, were obtained from the Harvard Brain Tissue Resource Center. Samples of normal control subjects were obtained from the Harvard Brain Tissue Resource Center and from the Department of Pathology, Yale University (Table S1). Cases with known or suspected

From the Child Study Center (JBL, GC, YK-S, TVF, DP, YL, JFL, FMV), Program in Neurodevelopment and Regeneration (JBL, GC, YK-S, DP, AH, FMV), Departments of Psychiatry (TVF) and Pathology (AH), Yale Kavli Institute for Neuroscience (NS, FMV), and Department of Neurobiology (MP, NS, FMV), Yale University School of Medicine, New Haven, Connecticut.

Authors JBL and GC contributed equally to this work.

Address correspondence to Flora M. Vaccarino, M.D., Yale University School of Medicine, Child Study Center, 230 South Frontage Road, New Haven, CT 06520; E-mail: flora.vaccarino@yale.edu.

Received Jan 8, 2014; revised Jul 4, 2014; accepted Jul 11, 2014.

neurological diseases and prolonged hypoxia were excluded. Four of the nine pairs were female subjects. There were no statistical differences in age, postmortem interval, or RNA quality between the TS and control groups (Table S1).

RNA Isolation, Library Construction, and Sequencing

Dissected regions were stored at -80°C until use, when sections were cut at $50\ \mu\text{m}$. During cryosectioning, prescoring the surface of the block every $150\ \mu\text{m}$ permitted separate collection of the caudate and putamen. Total RNA was isolated using RNeasy Plus Mini kit (Qiagen, Germantown, Maryland) according to the manufacturer's instruction, using 20 mg of tissue per genomic DNA eliminator column. RNA was assessed using Nanodrop spectrometer (Thermo Scientific, Suwanee, Georgia) and Bioanalyzer (Agilent Technologies, Wilmington, Delaware) to check quantity and quality. Paired-end complementary DNA libraries were prepared introducing a six-base sequence index into the adapter at the polymerase chain reaction (PCR) stage of sample preparation for Illumina multiplexed sequencing, according to the manufacturer's specification. Samples were sequenced using an Illumina Hi Seq2000 sequencing machine (Illumina, Inc., San Diego, California) to an average depth of 30 million reads per sample.

RNA-Seq Analyses

Tophat (20) was used to map the reads to the human genome (hg19) and the Gencode V7 (21) annotation. The resulting binary alignment/map (BAM) files were converted to sequence alignment/map (SAM) using SAMtools (22), sorted and converted to BED for transcript quantification in counts using BEDtools (23) and to mapped read format (MRF) for transcript quantification in reads per kilobase of transcript per million mapped reads (RPKM) using RSEQtools (24). We then used coverageBed in BEDtools to process the BED files and MRFquantifier in RSEQtools to process the mapped read format files. This resulted in estimated expression levels for about 36,000 genes.

Differential Expression

We used edgeR (25) to assess differential gene expression (DGE) at a false discovery rate (FDR) $<.05$. We accounted for matched pair design by using the generalized linear model capability of edgeR. Blocking was applied to individuals in the case of caudate- or putamen-specific differential expression analysis or to both individuals and regions in the case of the analysis of the full dataset. See [Supplementary Methods in Supplement 1](#) for more details.

Co-expression Network Analysis

We used the Weighted Gene Co-expression Network Analysis (WGCNA) package (26). The analysis produced a network of 20 modules, corresponding to about 12,000 genes. Permutation analysis was used to verify the modules' genes to be co-expressed beyond chance. The WGCNA function `userListEnrichment` was used to test the modules for overrepresentation in BrainLists, DGE, and copy number variants (CNVs) (see [Supplementary Methods in Supplement 1](#) for details).

Gene Set Enrichment Analysis

We used the Gene Set Enrichment Analysis (GSEA) package (27) to identify the WGCNA modules that were enriched in differentially expressed genes (DEGs). The gene expression matrix was used as input to the package, normalizing the RPKM data by \log_2 (i.e., $\log_2[\text{RPKM} + .5]$) transformation. The network modules were used as

test gene sets, according to the format required by the package. The cutoff for significant enrichment was FDR q value $<.05$.

Functional Enrichment Analysis

Ingenuity Pathway Analysis (IPA) (Ingenuity Systems, Redwood City, California; www.ingenuity.com) and ConsensusPathDB (28) were used to test differentially expressed genes and WGCNA modules for overrepresentation in Gene Ontologies, Canonical Pathways, Upstream Regulators, and Networks.

Sample Clustering

The function `heatmap.2` was used to make the heat map in [Figure S1](#). We used the Canberra method within the distance function. The DESeq package (29) normalization protocol for count data was used for hierarchical clustering.

Quantitative Real-Time Polymerase Chain Reaction Validation

RNA was reverse transcribed using SuperScript III (Life Technologies, Grand Island, New York), and expression levels were evaluated with Applied Biosystems OneStep (Life Technologies) quantitative real-time PCR (qPCR) using SYBR Power Green master mix and a standard protocol that included melting curve analysis. The raw data were normalized to the geometric mean of two reference genes, *GAPDH* and *IPO8*. Differential gene expression was determined using the ddCt method (30,31). Genes chosen for validation included randomly selected genes, as well as cholinergic-related and inflammatory/immune response-related genes. Primers are listed in [Table S2](#).

Immunohistochemistry

Formalin-fixed tissue samples from the basal ganglia were sectioned at $50\ \mu\text{m}$ and processed for nitric oxide synthase 1 (NOS1), CD45RO (protein tyrosine phosphatase, receptor type, C [PTPRC]), and ionized calcium-binding adapter molecule 1 (IBA) immunostaining as previously described (19). Cell numbers were estimated by stereological analyses using Stereoinvestigator (MicroBrightField, Williston, Vermont) as previously described (19). See [Supplementary Methods in Supplement 1](#) for more details.

Results

Differentially Expressed Genes in the Basal Ganglia in TS

Whole genome transcripts in the caudate and putamen of nine TS subjects and nine matched normal control subjects (Table S1) were obtained by RNA-Seq and analyzed for differences between patients and control groups using DGE and co-expression network analysis; for an overview, see [Figure 1](#). DGE analysis of the combined caudate and putamen dataset (considering $n = 9$ matched pairs, blocking for individual pairs and for region within each pair; see Methods and Materials) revealed 1131 genes differentially expressed between TS and NC, of which 309 were downregulated and 822 were upregulated (FDR $<.05$; [Table S3a](#)). Unsupervised hierarchical clustering of the top 100 differentially expressed genes revealed co-regulated patterns of gene expression across samples with segregation of TS and NC, independent of postmortem interval, RNA quality, medication use, and other confounding variables ([Figure S1](#)). Only a single TS subject (TS4) more closely resembled the NCs in the unsupervised hierarchical clustering analysis. This subject had no first-degree relatives with TS but did have a positive history for a number of perinatal risk factors. This observation again provides clear evidence for heterogeneity in the

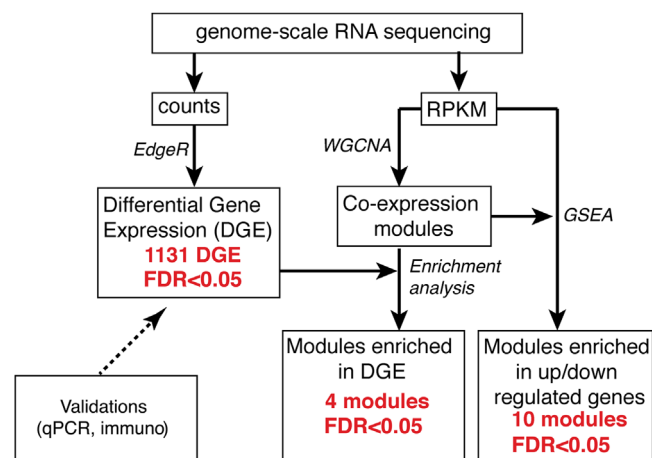


Figure 1. General scheme of our analyses. Analysis flow diagram for RNA-Seq data analysis. Boxes: preanalysis and postanalysis data; arrows: methods applied to preanalysis data to get postanalysis data/results. Red text: results. RNA-Seq reads are converted into read counts and the reads per kilobase of transcript per million mapped reads, or RPKM, for each transcript in the Gencode annotation. EdgeR is applied to counts to infer differential gene expression (DGE). Weighted Gene Co-expression Network Analysis, or WGCNA, in combination with Gene Set Enrichment Analysis, or GSEA, is applied to RPKM to infer modules of co-expressed genes enriched in differentially expressed genes. FDR, false discovery rate; immuno, immunohistochemistry; qPCR, quantitative real-time polymerase chain reaction.

pathobiology and etiology of TS. Validation by qPCR showed the same direction fold change for 13 of 13 genes examined with an overall correlation of .88 between qPCR and DGE; p value: 6.4×10^{-5} (Figure S2).

Table 1. Hand-Curated Subset of Differentially Expressed Genes

		FC	FDR
Cholinergic			
<i>CHAT</i>	Choline O-acetyltransferase	-2.31	1.39E-07
<i>CHRM2</i>	Cholinergic receptor, muscarinic 2	-1.99	4.32E-04
<i>SLC18A3</i>	Solute carrier family 18 (vesicular acetylcholine), member 3	-2.17	4.04E-05
<i>SLC5A7</i>	CHT1; solute carrier family 5 (choline transporter), member 7	-2.55	6.65E-08
<i>LHX8</i>	LIM homeobox 8	-1.90	1.39E-03
<i>NTRK1</i>	Neurotrophic tyrosine kinase, receptor, type 1	-1.91	1.17E-03
<i>GBX2</i>	Gastrulation brain homeobox 2	-1.65	4.23E-02
GABAergic			
<i>GAD1</i>	Glutamate decarboxylase 1 (brain, 67 kDa)	-1.64	1.21E-02
<i>GABRA1</i>	Gamma-aminobutyric acid A receptor, alpha 1	-1.47	2.31E-02
<i>GABRA3</i>	Gamma-aminobutyric acid A receptor, alpha 3	-1.96	5.85E-04
<i>GABRG2</i>	Gamma-aminobutyric acid A receptor, gamma 2	-1.50	2.61E-02
<i>GABRQ</i>	Gamma-aminobutyric acid A receptor, theta	-1.82	1.11E-02
<i>NOS1</i>	Nitric oxide synthase 1 (neuronal)	-1.58	6.40E-03
<i>NPY</i>	Neuropeptide Y	-1.66	8.15E-03
<i>NPY2R</i>	Neuropeptide Y receptor Y2	-2.81	2.33E-04
<i>SST</i>	Somatostatin	-1.59	4.42E-03
Dopaminergic			
<i>DRD1</i>	Dopamine receptor D1	-1.50	3.20E-02
<i>DRD5</i>	Dopamine receptor D5	-2.10	2.47E-03
Others of Interest			
<i>SLITRK5</i>	SLIT and NTRK-like family, member 5	-1.54	1.08E-02
<i>OPRK1</i>	Opioid receptor, kappa 1	-1.60	3.48E-02
<i>OPRM1</i>	Opioid receptor, mu 1	-1.43	4.03E-02
<i>HTR2C</i>	5-hydroxytryptamine (serotonin) receptor 2C, G protein-coupled	-1.62	7.44E-03

Genes are listed under each category they represent, along with fold change and FDR corrected p values. FC, fold change; FDR, false discovery rate.

Downregulation of Transcripts Involved in Neuronal Signaling, Specifically Striatal Interneurons

Functional annotation of the downregulated genes by IPA revealed a signature of neuronal signaling dysfunction in the striatum of TS individuals (Tables S4 and S5). In the striatum, projection neurons of the direct and indirect pathways comprise at least 70% to 80% of all neurons (32,33). The striatum also has four types of interneurons: the tonically active cholinergic neurons, and three classes of GABA interneurons, expressing NOS1/neuropeptide Y (NPY)/somatostatin (SST), parvalbumin (PVALB), or CALRETININ (CALB2 or CR) (34,35). To find out whether transcript downregulation was specific for particular neuron types, we performed manual classification of the DGE according to neurotransmitter class (Table 1). Genes encoding for abundant neuropeptides expressed by striatal projection neurons, such as prodynorphin and tachykinin precursor 1, were not changed, whereas there was significant downregulation for genes related to cholinergic interneurons, including acetylcholine neurotransmitter synthesis and transport (*CHAT*, *SLC5A7*, *SLC18A3*), cholinergic receptors (*CHRM2*), and the homeodomain genes *LHX8* and *GBX2*, critical for the development of forebrain cholinergic neurons (36–38) (Table 1). Several genes related to striatal GABAergic interneurons also showed reduced expression, including *NOS1*, *NPY*, and *SST* but not *PVALB*, *CALB2/CR* (Table 1).

Previously, we reported decreased numbers of cells immunostained for *CHAT* and *PVALB* in the striatum of TS; however, *NOS1*/*NPY*/*SST* interneurons were not assessed (19). Hence, we quantified the density of immunohistochemically identified *NOS1*⁺ cells in series of postmortem tissue sections from seven TS and seven control cases, three of which were new cases and four that had been also evaluated using RNA-Seq. We found a significant decrease in *NOS1*⁺ interneurons both in the caudate (–37.6%,

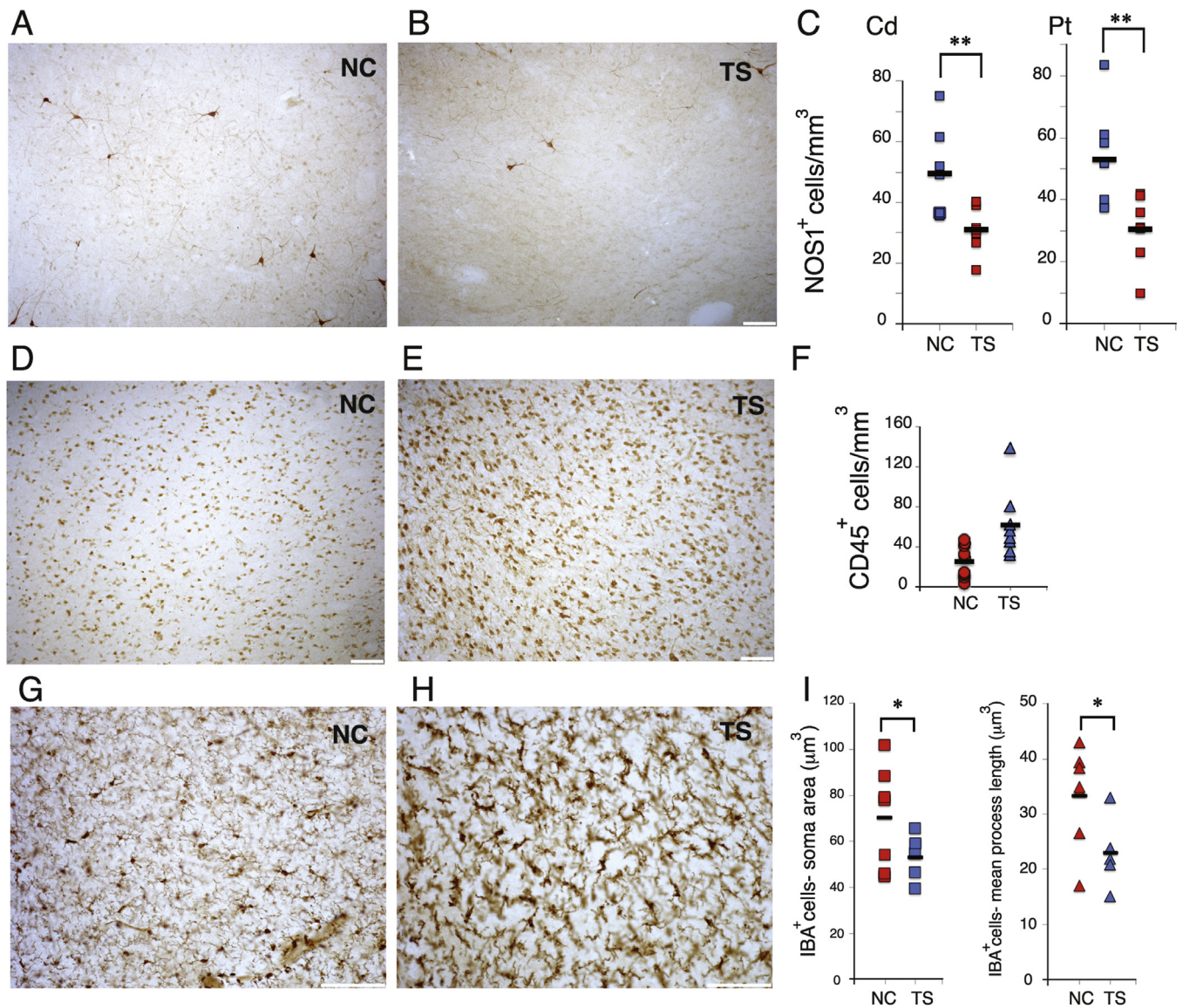


Figure 2. Differential nitric oxide synthase 1 (NOS+) cell density, elevated protein tyrosine phosphatase, receptor type, C (CD45/PTPRC) cell density, and microglial activation in Tourette syndrome (TS) patients. **(A–C)** Immunostaining for NOS⁺ cells in the caudate of representative normal control (NC) **(A)** and TS cases **(B)**. Scale bars 100 μm. **(C)** Stereological estimates of NOS⁺ cell density (cells per mm³) in the caudate and putamen of normal control ($n = 7$) and TS ($n = 7$) cases. **(D–F)** Immunostaining for CD45/PTPRC⁺ cells in the caudate of representative normal control **(D)** and Tourette syndrome cases **(E)**. Scale bars 100 μm. **(F)** Stereological estimates of PTPRC⁺ cell density (cells per mm³) in the caudate of control ($n = 10$) and TS ($n = 8$) cases. **(G–I)** Immunostaining for ionized calcium-binding adapter molecule 1 (IBA⁺) cells in caudate of representative normal control **(G)** and Tourette syndrome cases **(H)**. Scale bars 100 μm. **(I)** IBA⁺ cell body size (μm²) and dendrite length (μm) in the caudate in control ($n = 7$) and TS ($n = 5$) cases. * $p < .05$, ** $p < .01$ one-tailed Student t test. Cd, caudate; Pt, putamen.

$p = 1.25E-2$) and in the putamen (-42.2% , $p = 1.24E-2$) of TS versus control subjects (Figure 2A–C), confirming the transcriptome analyses. No significant change in PVALB transcripts was detected in the transcriptome. However, we detected a 75% decrease in messenger RNA for potassium voltage-gated channel subfamily C member 1 (*KV3.1*) (*KCNC1*) approaching statistical significance (FDR = $6.8E-2$). *KCNC1* is a potassium channel selectively expressed by PVALB interneurons that confers fast re-polarization and high firing properties typical of these cells (39–42). Additional GABAergic signaling genes downregulated in TS included the GABA synthetic enzyme glutamate decarboxylase 1 (*GAD1*) and several GABAergic receptor subunits (Table 1).

Upregulation of Transcripts and Proteins Related to the Monocyte/Microglia Lineage

Functional annotation of the genes upregulated in TS by IPA revealed inflammatory response and immune cell development and trafficking signatures (Tables S4 and S5). Upregulated transcripts included tumor necrosis factor alpha, interleukin (*IL*)-6, and *IL-12*, previously found altered in TS in peripheral studies (43); toll-like receptors that modulate regulatory T cell function; several major histocompatibility complex class II molecules; immunoglobulin chains; and several chemokine (C-C motif) receptor tumor necrosis factor-, and *IL*-family cytokines that have been implicated in autoimmune disorders. Pathway analysis conducted with

MetaCore (Thomson Reuters, New York, New York) yielded results similar to IPA for both upregulated and downregulated transcripts (Table S6).

We considered the possibility that an infiltrate of immune cells from the periphery might explain the upregulation of immune transcripts in brain. However, the transcriptome data did not show a significant upregulation of B cell and T cell specific transcripts, whereas the messenger RNA for phosphotyrosine phosphatase C (*CD45/PTPRC*), a transcript expressed by all differentiated hematopoietic cells including lymphocytes, monocytes, and macrophages (44), was increased by approximately twofold in TS brains (Table S3c). We examined *PTPRC*⁺ cells in the caudate of TS and control brains by immunohistochemistry. We found a significant increase in density of *PTPRC*⁺ cells in TS (+153%, $p = 7.30E-3$) (Figure 2D–F). As several microglia-related transcripts (*IBA*, *CD68*) were upregulated in TS subjects, we considered that increased number of cells of the macrophage/microglia lineage might be underlying the inflammatory changes. Evaluation of IBA protein expression in the caudate revealed no change in the density of IBA⁺ cells (data not shown). However, we found a significant decrease in IBA⁺ cell body size ($p = 1.27E-2$) and process length ($p = 2.53E-2$), indicative of microglia activation (Figure 2G–I). Together, the results suggest that the primary source of inflammation may be activated brain microglia, although we cannot exclude the involvement of other cells, i.e., peripheral monocytes.

We next intersected our 1131 DEGs with existing microarray transcriptome studies, three in blood (45–47) and one in the putamen (48). We found that not much overlap exists between our DGE discovered by RNA-Seq and previous microarray studies in TS tissue. Of the 10 genes found to be nominally differentially expressed in the putamen of three TS brains in the Hong *et al.* study (48) (see their Table 4), only *PTP4A3* was significantly changed in our dataset, and of the 13 genes found to be nominally differentially expressed in the TS blood by exon array (49) (see their Supplemental Table 1 and Supplemental Table 2), only one gene, *MYO7A*, intersected with our dataset. None of the 51 genes nominally differentially expressed in the second blood study (46) (see their Supplemental Table 1) intersected with our dataset. Finally, of the 14 genes significantly differentially expressed in the third TS blood study (45) (see their Table 1), only one gene, *LILRA3*, intersected with our 1131 DEGs.

Differentially Expressed Genes in the Caudate and Putamen in TS

In addition to performing a combined analysis, we also analyzed separately the caudate and putamen to identify possible region-specific contributions to the overall signature. We found 434 DEGs in the caudate and 368 in the putamen (FDR < .05; Table S3b and c). Intersection of the DEGs between the caudate and putamen (see Venn Diagram in Figure S3) revealed 198 DEGs specific to the caudate and 132 specific to the putamen (Table S7a), hinting at a possible differential regional involvement of these regions in the disease. Functional analysis of the region-specific lists (listed in Table S7a) showed strong involvement of the caudate-specific DEGs in immunological disease, inflammatory response, cell-to-cell signaling and interaction (Table S7b) and a moderate involvement of the putamen-specific DEGs in neurological disorders, cell-to-cell signaling/interaction, and tissue morphology (Table S7c). However, intersection of the DEGs from the caudate, putamen, and combined analysis (see Venn Diagram in Figure S3) revealed that analyzing the caudate and putamen in isolation, as compared with the overall combined analysis,

identifies, respectively, only 18 and 27 DEGs (Figure S3), suggesting that the combined analysis captures most of the individual region DEGs and, as expected, produces about 600 to 700 more DEGs as a consequence of the increased power, thus allowing more discovery. In conclusion, while the difference in DEGs between caudate and putamen may be a true biological signature, we cannot rule out the possibility of a statistical artifact due to lower number of samples. We therefore focus on the combined dataset throughout the rest of this article.

Co-expression Network Analysis

Preliminary analyses suggested that the level of gene expression for *CHAT* was strongly correlated with that of other cholinergic genes (Pearson's mean $r = .71$), as well as with GABAergic genes (Pearson's mean $r = .74$), including *GAD1*, several GABA receptor subunits, *NOS1*, *NPY*, and *SST*, across all TS subject and control subjects. In contrast, the correlation between *CHAT* and immune system-related transcripts displayed a poor correlation coefficient (Pearson's mean $r = .16$) (Figure S4).

We next used network inference and analysis to explore in an unbiased fashion correlations among transcripts that may provide clues to disease pathogenesis. To this end, we applied WGCNA (26) to the entire transcriptome dataset (see Figure 1 for an overview of the analyses). This analysis yielded 20 modules where transcripts in each module were significantly correlated in overall pattern of expression across all samples. After permutation analysis, 17 modules of co-expressed genes remained significant (FDR < .05; Table S8).

To test whether the WGCNA modules were differentially expressed between TS and NC, we performed GSEA (27), where the modules were used as test gene sets and gene expression levels were used as input. Ten modules were significantly enriched in upregulated or downregulated genes (Table 2; Table S9). Their member genes, together with their fold change in expression in TS versus control subjects from DGE analysis, are listed in Table S10. Two modules, magenta and turquoise, were the top scoring upregulated and downregulated modules by GSEA normalized enrichment score (Table S9). As expected, the magenta and turquoise modules showed the strongest statistical overlap with the upregulated and downregulated genes resulting from DGE analysis: 297 of the 822 upregulated genes were in the magenta module ($p = 2.5E-318$), while 116 of the 309 downregulated genes were in the turquoise module ($p = 3.4E-43$) (Table S11).

We next examined the biological role of the 10 differentially expressed modules by enrichment analysis for brain-related cell types and diseases using the BrainLists database from WGCNA, as well as for Gene Ontology and Canonical Pathways categories using GO:Biofunctions, CP:KEGG, and CP:Reactome from ConsensusPathDB (28). The modules' biological classifications are summarized in Table 2 and described in detail in Tables S12 and S13. There were two neuronal modules, turquoise and blue, which were the two top scoring downregulated modules in TS. The turquoise module was enriched in PVAlb cell type categories and various neurotransmission-related biofunctions (i.e., glutamatergic, dopaminergic, GABAergic, and cholinergic synapses, calcium and potassium channels); indeed, the majority of the striatal interneuron-related transcripts in Table 1 are members of the turquoise module. The blue module was enriched in cellular catabolic pathways and protein ubiquitination. The magenta module, the top scoring for upregulated genes, was enriched in microglia cell type categories and immune-related pathways. There were two astrocyte modules, the purple and the lightcyan; the first was enriched in cell adhesion and astrocyte-related

Table 2. Biological Classification for the Modules Significantly Enriched in Differentially Expressed Genes

Module Name/Downregulated/ Upregulated	Biological Classification	Database	Corrected <i>p</i> Values
Turquoise (Down)	Neuron_probable__Cahoy	BrainLists	3.33E-267
	Synaptic transmission	GO:Biofunctions	2.96E-81
	Glutamatergic synapse – Homo sapiens	CP:KEGG	2.87E-14
Blue (Down)	blue_M16_Neuron__CTX	BrainLists	6.71E-79
	Cellular metabolic process	GO:Biofunctions	6.62E-21
Pink (Down)	Ubiquitin mediated proteolysis – Homo sapiens	CP:KEGG	8.23E-05
	DownWithAlzheimers_Liang__ADvsCT_inCA1	BrainLists	1.42E-12
	Nucleic acid metabolic process	GO:Biofunctions	5.53E-26
Green (Down)	Gene Expression	CP:Reactome	1.35E-17
	turquoise_M14_Nucleus__HumanMeta	BrainLists	8.90E-30
	Cellular macromolecule metabolic process	GO:Biofunctions	2.72E-10
Brown (Down)	Spliceosome – Homo sapiens	CP:KEGG	2.83E-06
	brown_M3_Astrocytes__HumanMeta	BrainLists	2.79E-03
	Nucleic acid metabolic process	GO:Biofunctions	4.63E-27
Lightcyan (Down)	Gene Expression	CP:Reactome	1.45E-08
	Astrocyte_probable__Cahoy	BrainLists	1.43E-02
	Homophilic cell adhesion	GO:Biofunctions	2.80E-20
Tan (Down)	Signaling by NOTCH	CP:Reactome	9.37E-04
	blue_M2_Oligodendrocytes__HumanMeta	BrainLists	9.82E-127
	Ensheathment of neurons	GO:Biofunctions	3.86E-08
Red (down)	Metabolism of lipids and lipoproteins	CP:Reactome	2.76E-02
	NA	BrainLists	NA
	Nucleobase-containing compound biosynthetic process	GO:Biofunctions	8.12E-15
Magenta (Up)	Generic Transcription Pathway	CP:Reactome	8.51E-11
	pink_M10_Microglia(Type1)__HumanMeta	BrainLists	1.29E-107
	Immune response	GO:Biofunctions	5.40E-79
Purple (Up)	Staphylococcus aureus infection - Homo sapiens	CP:KEGG	2.02E-29
	Astrocyte_probable__Cahoy	BrainLists	2.90E-49
	Cell adhesion	GO:Biofunctions	4.43E-06
	Propanoate metabolism – Homo sapiens	CP:KEGG	1.11E-02

Modules are shown in decreasing order of GSEA normalized enrichment score (see [Supplementary Table S8](#)) for each of the downregulated or upregulated groups. The Biological Classification column lists the most significant lists from overrepresentation analysis using list categories shown in the Database column. Their sources are WGCNA for BrainLists and ConsensusPathDB (28) for GO:Biofunction and Canonical Pathways. Corrected *p* value: FDR corrected *p* values.

CP, Canonical Pathways; FDR, false discovery rate; GO, Gene Ontology; GSEA, Gene Set Enrichment Analysis; NA, not applicable; WGCNA, Weighted Gene Co-expression Network Analysis.

metabolic pathways, whereas the second was enriched in protocadherin-gamma molecules (Table 2 and Tables S12 and S13).

To understand whether the DGE genes impact specific subgroups or more connected genes within modules, we estimated the gene scaled intramodular connectivity (26) and on this basis determined the 10 genes that were most connected to all the other genes within each module (hub genes) (shown in the center of each module in Figure 3). We found that the microglia/immune module (magenta) is perturbed dramatically at gene expression level, with many highly interconnected genes, including the hub genes, being overexpressed (Figure 3, red color). Conversely, the gene expression changes in the turquoise, blue, lightcyan, and purple modules involved nonhub, less interconnected genes (Figure 3, red and blue colors for overexpressed and underexpressed genes, respectively).

Lack of Correlation between Interneuron-Related and Immune-Related Gene Expression

To reveal how modules interact within the network, we first computed the eigengene, which is the first principal component of a module's member genes expression levels. We then applied hierarchical clustering to the 17 modules' eigengenes (Figure S5) and found that the two astrocytes modules, lightcyan and purple,

formed a distinct group. Furthermore, the two neuronal modules, turquoise and blue, enriched in interneuron and neuronal catabolism biofunctions, respectively, clustered together, whereas the microglial module (magenta) significantly correlated with the nucleus (green), transcription (red), and oligodendrocyte (tan) modules but was quite independent from the neuronal and astrocyte modules. This confirms the previous suggestion that the immune response may be decoupled from the changes in interneurons. The overall network between the modules, where the nodes are modules and edges are the significant correlations, is represented in the center of Figure 3.

Significant Overlap of Genes Revealed by Co-expressed Network Analysis with Previous TS Genomic Study

To gain further insights into the present findings on the transcriptome, we overlapped our DGE and WGCNA findings with the list of genes intersecting rare CNVs from a family-based TS study (50). We first intersected the CNV genes from the TS group with the ones from the NC group, identified the common genes, and generated a list of TS-specific, NC-specific, and common CNV genes, which we then used for subsequent analysis. We found that only the TS-specific CNV genes, and none of the common or NC-specific genes, overlapped with our datasets. Remarkably,

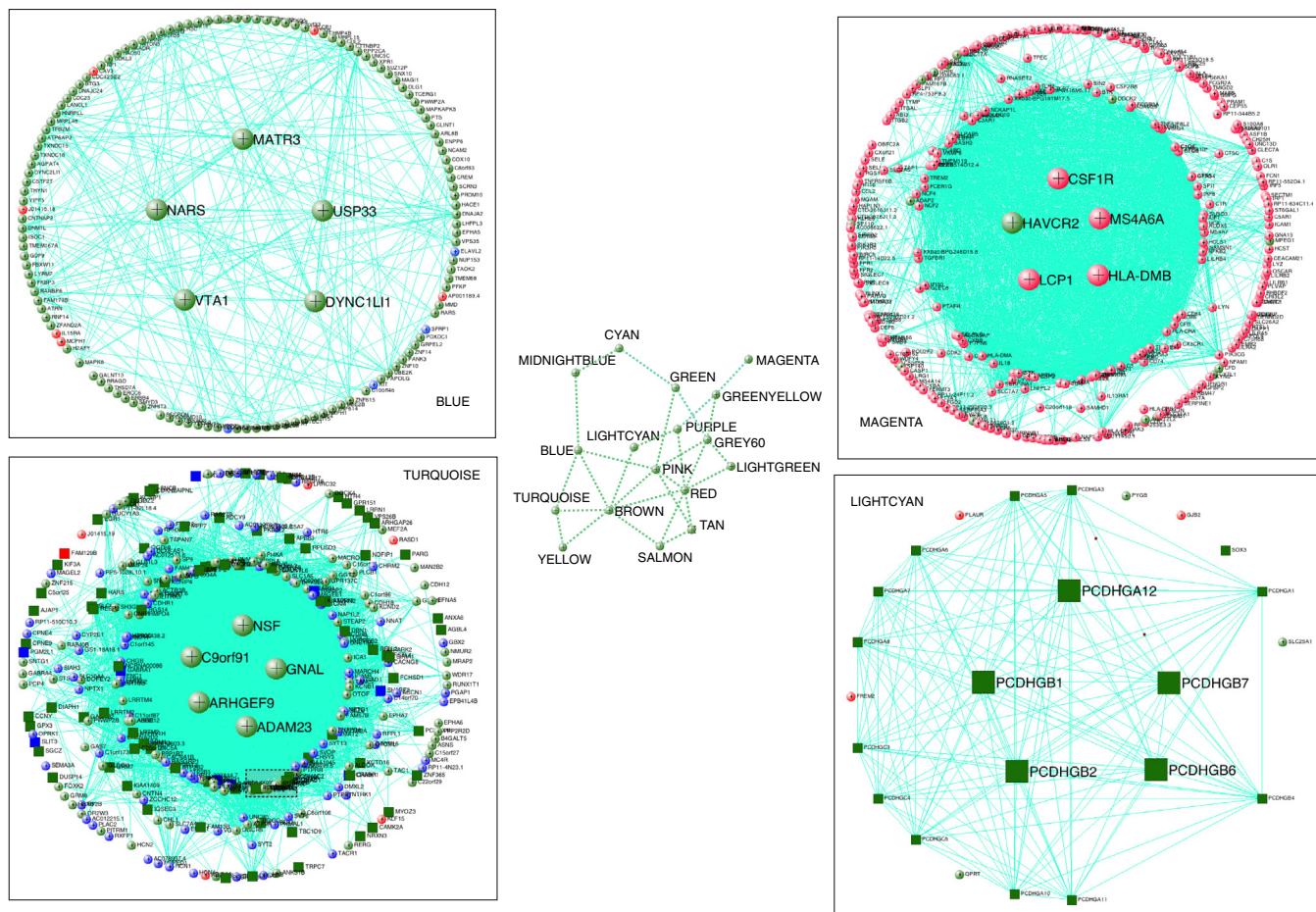


Figure 3. Differentially co-expressed gene networks in Tourette syndrome. The center of the figure shows the global network where the nodes (green circles) are Weighted Gene Co-expression Network Analysis modules and the edges are significant correlations between the modules eigengenes. The four inserts show the detailed network within four relevant modules. Top left: blue (neuronal metabolism) module. Top right: magenta (immune/microglia) module. Bottom right: lightcyan (cell adhesion/protocadherin) module. Bottom left: turquoise module (synaptic transmission/interneuron). Circles: network genes. Large circles: top five genes with highest intramodular connectivity (hubs). Squares: network genes overlapping with copy number variant genes. Red: upregulated gene. Blue: downregulated gene. Concentric circle arrangement in the case of the turquoise (bottom left) and magenta (top right) modules reflects intramodular connectivity: genes closer to the center have higher intramodular connectivity than genes further away from the center.

only the turquoise (interneurons) and the lightcyan (protocadherin-gamma/cell adhesion) modules significantly overlapped with TS-specific CNV genes ($p < 3.1E-3$ and $p < 3.1E-8$, respectively), whereas no enrichment was found for any other module, including the magenta, which was the top-scoring module for upregulated genes. The TS CNV genes in the lightcyan module intersected the gamma-protocadherin hub genes (Figure 3, squares). In contrast, CNVs in the turquoise module involved more peripheral, less interconnected genes (Figure 3, squares); however, differently than the lightcyan, these CNVs genes included many genes that were differentially expressed (blue and red squares), suggesting significant convergence of DGE, gene network, and CNV analyses in the turquoise module.

Discussion

Here, we performed the first unbiased and comprehensive characterization of gene expression changes in the basal ganglia of patients with TS. We identified 1131 differentially expressed genes in the striatum of individuals with lifelong TS. In comparison, fewer differentially expressed genes were found when

caudate and putamen were analyzed separately, and even fewer were specific to each region, suggesting that biological changes are mostly shared across the striatum. We were unable to confirm that transcripts previously found to be nominally differentially expressed in the blood in a subset of TS subjects were differentially expressed in the basal ganglia of the nine subjects included in this study. The observed lack of overlap with previous studies in blood further stresses the need to analyze brain samples, as opposed to blood samples (45–47). There was only one gene overlapping with a previous microarray study of the TS putamen, where 10 genes were nominally differentially expressed in three TS subjects (48), possibly reflecting the low sample size of their study. Interestingly, we obtained a much higher yield in differential gene expression despite a still limited number of brain samples ($n = 9$ matched pairs, two regions each). This reflects, in part, the careful sample selection and experimental design and, in part, the increased power of RNA-Seq over microarray analyses. Co-expression network analysis, a well-known and established data reduction technique, also addresses power issues, by reducing the dimensionality of the problem from tens of thousands of genes to a few modules of co-expressed genes. The fact that our results are consistent across different, yet

complementary, data analytical approaches (i.e., DGE and WGCNA) supports the idea that the number of samples in our study is sufficient to infer differences between the Tourette and NC. Hierarchical clustering revealed segregation of gene expression differences according to diagnosis but not drug treatment, comorbidities, postmortem interval, and RNA quality. Nevertheless, the small sample size limited our ability to control for these variables and future studies will need to consider these potentially confounding factors. Notably, our correlation between qPCR and RNA-Seq was close to .9, in good agreement to previous comparative reports of the two methods, wherein correlation analysis and sometimes additional validation subjects were employed due to the intrinsic higher variability of qPCR assays (51–54).

WGCNA identified eight downregulated modules and two upregulated modules in TS. The two top-scoring downregulated, turquoise and blue, were characterized, respectively, by interneuron signaling and neuronal catabolic pathways. The two upregulated modules, magenta and purple, were characterized, respectively, by microglia signaling and astrocyte metabolic pathways (Table 2). The fact that the turquoise module, enriched for genes critical for neurotransmitter production, signaling, and function of cholinergic and GABAergic interneurons, was the most significantly enriched in downregulated genes is consistent with immunohistochemical findings suggesting that striatal interneuron proteins are decreased in TS. While two of these classes of interneurons were previously reported to be decreased in TS based on antibody labeling of one or two identifying proteins (19), the current data show that multiple genes involved in the comprehensive function of these cells are decreased, providing the first confirmation that indeed cholinergic and GABAergic interneurons may be functionally immature or missing in TS. Although GABA interneurons represent less than 4% of the total neuron population in the striatum (19,55,56), they exert a prominent role in feed-forward inhibition driven by corticostriatal input, which predicts that their reduction can result in severe disruptions to cortically driven internal striatal activity and ultimate circuit output (57,58).

Unexpectedly, a module greatly enriched in inflammatory response transcripts (magenta) was the most significantly enriched in upregulated genes. This finding is intriguing, given previous reports describing peripheral immunological changes in TS patients (43,59–62). It is important to note that the cases used in this study did not meet criteria for pediatric autoimmune neuropsychiatric disorders associated with streptococcal infection (63–65) or pediatric acute onset neuropsychiatric syndrome (66–68). We did not find any evidence for a white cell infiltrate in brain tissue, but rather, the changes were consistent with a macrophage/monocyte mediated inflammatory response, supported by an increase in cells positive for the generic marker PTPRC and local reactive microglia within the brain.

A possible hypothesis linking the above findings is that an intrinsically upregulated immune response in striatal tissue is the cause of the neuronal dysfunction, either because interneurons may be directly killed by the immune cells or because of secondary inflammatory alterations. Another possibility is that immune activation would be the consequence of neuronal dysfunction, i.e., secondary to interneuron death. Against both hypotheses is the fact that the transcripts in the magenta microglial module were not correlated with those in the turquoise interneuron module, suggesting that the immune and neuronal events were not causally related to each other. Instead, the magenta module was most correlated with two modules with “nucleus” and “transcription” functional annotations, whereas the

turquoise neuronal module was most correlated with the other neuronal module (blue), functionally annotated by catabolic pathways and protein ubiquitination suggesting that neuronal demise may be secondary to metabolic alterations.

Interestingly, only the turquoise interneuron module and lightcyan protocadherin module (but not the magenta immune module) were significantly enriched in genes implicated in the etiology of TS by the largest CNV study published in TS patients to date (50). These two modules, however, are not correlated with each other: the turquoise is most correlated with the blue neuronal catabolism module, as mentioned above, while the lightcyan module is most correlated with the other astrocyte module (purple), which is enriched in organic acid metabolism as well as cell adhesion (Table S13), suggesting a unique role for astrocytes in TS pathogenesis. Furthermore, differently than in the lightcyan module, the CNV genes in the turquoise module include many differentially expressed neurotransmitter-related transcripts (i.e., *CHAT*, several GABA receptors, and the high affinity choline transporter). This convergence again emphasizes that genes in the turquoise module may provide fundamental clues in TS etiology/pathogenesis. The microglia/immune module (magenta) had widespread perturbation in gene expression levels, including many hub genes, yet lacked overlap with CNV genes. This may reflect a downstream effect of the disease, although it cannot be excluded that any undetected genetic defect may be present at the level of the regulators of transcripts within this module. Overall, the lack of correlation between the magenta and the other differentially expressed modules that are enriched in genes overlapping with CNVs suggests that immune and neuronal events are not pathophysiologically dependent on each other; however, we cannot exclude that a previous relationship might have existed developmentally. Specifically, it is worth noting that microglia are intimately involved in circuit formation during central nervous system development and circuit refinement (69).

In summary, a convergence of results from DGE and network analyses of the present transcriptome data, together with CNVs previously implicated in TS, strongly implicates disrupted basal ganglia neuronal signaling, particularly interneurons (i.e., cholinergic and NOS1^+ -GABAergic populations) in the pathophysiology of severe, persistent TS and suggests that metabolic alterations may be linked to their death or dysfunction. Concomitantly, but decoupled from the neuronal changes, we found a significant increase in immune and inflammatory transcripts that appear to be endogenous to the central nervous system. Developmentally relevant modeling may help us to untangle the cause-effect mechanisms underlying these phenomena.

This work was supported by grants from the National Tourette Syndrome Association, the National Institutes of Health (NS054994 to FMV and MH081896 to NS), and from the Brain and Behavior Research Foundation (National Alliance for Research on Schizophrenia and Depression) to FMV. YK-S is currently affiliated with the Department of Neural Regenerative Medicine, Sapporo Medical University School of Medicine, Sapporo, Japan. DP is currently affiliated with the Institute of Mathematics and Informatics, Bulgarian Academy of Sciences, Sofia, Bulgaria.

We acknowledge Yuka Imamura-Kawasawa for her technical advice on RNA isolation; the National Tourette Syndrome Association, George Tejada, Louis Fernandes, and the Harvard Brain Tissue Resource Center for providing Tourette and control tissue; and Nancy Thompson for help with the clinical phenotyping. The Harvard Brain Tissue Resource Center is supported in part by National Institutes of Health Grant R24 MH068855.

Dr. Leckman has received support from the following: National Institutes of Health (salary and research funding), Tourette Syndrome, Grifols (research funding), Klingenstein Third Generation Foundation (medical student fellowship program), John Wiley and Sons (book royalties), McGraw Hill (book royalties), and Oxford University Press (book royalties). All other authors report no biomedical financial interests or potential conflicts of interest.

Supplementary material cited in this article is available online at <http://dx.doi.org/10.1016/j.biopsych.2014.07.018>.

- Leckman JF (2002): Tourette's syndrome. *Lancet* 360:1577–1586.
- Price RA, Kidd KK, Cohen DJ, Pauls DL, Leckman JF (1985): A twin study of Tourette syndrome. *Arch Gen Psychiatry* 42:815–820.
- The Tourette Syndrome Association International Consortium for Genetics (1999): A complete genome screen in sib pairs affected by Gilles de la Tourette syndrome. The Tourette Syndrome Association International Consortium for Genetics. *Am J Hum Genet* 65:1428–1436.
- Scharf JM, Yu D, Mathews CA, Neale BM, Stewart SE, Fagerness JA, *et al.* (2013): Genome-wide association study of Tourette's syndrome. *Mol Psychiatry* 18:721–728.
- Ercan-Sencicek AG, Stillman AA, Ghosh AK, Bilguvar K, O'Roak BJ, Mason CE, *et al.* (2010): L-histidine decarboxylase and Tourette's syndrome. *N Engl J Med* 362:1901–1908.
- Abelson JF, Kwan KY, O'Roak BJ, Baek DY, Stillman AA, Morgan TM, *et al.* (2005): Sequence variants in SLITRK1 are associated with Tourette's syndrome. *Science* 310:317–320.
- Mathews CA, Bimson B, Lowe TL, Herrera LD, Budman CL, Erenberg G, *et al.* (2006): Association between maternal smoking and increased symptom severity in Tourette's syndrome. *Am J Psychiatry* 163:1066–1073.
- Hoekstra PJ, Dietrich A, Edwards MJ, Elamin I, Martino D (2013): Environmental factors in Tourette syndrome. *Neurosci Biobehav Rev* 37:1040–1049.
- Martino D, Dale RC, Gilbert DL, Giovannoni G, Leckman JF (2009): Immunopathogenic mechanisms in tourette syndrome: A critical review. *Mov Disord* 24:1267–1279.
- Elamin I, Edwards MJ, Martino D (2013): Immune dysfunction in Tourette syndrome. *Behav Neurol* 27:23–32.
- Stern E, Silbersweig DA, Chee KY, Holmes A, Robertson MM, Trimble M, *et al.* (2000): A functional neuroanatomy of tics in Tourette syndrome. *Arch Gen Psychiatry* 57:741–748.
- Peterson BS, Thomas P, Kane MJ, Scahill L, Zhang H, Bronen R, *et al.* (2003): Basal ganglia volumes in patients with Gilles de la Tourette syndrome. *Arch Gen Psychiatry* 60:415–424.
- Sowell ER, Kan E, Yoshii J, Thompson PM, Bansal R, Xu D, *et al.* (2008): Thinning of sensorimotor cortices in children with Tourette syndrome. *Nat Neurosci* 11:637–639.
- Tobe RH, Bansal R, Xu D, Hao X, Liu J, Sanchez J, Peterson BS (2010): Cerebellar morphology in Tourette syndrome and obsessive-compulsive disorder. *Ann Neurol* 67:479–487.
- Bloch MH, Leckman JF, Zhu H, Peterson BS (2005): Caudate volumes in childhood predict symptom severity in adults with Tourette syndrome. *Neurology* 65:1253–1258.
- Albin RL, Mink JW (2006): Recent advances in Tourette syndrome research. *Trends Neurosci* 29:175–182.
- Vaccarino F, Kataoka Y, Lenington J (2013): Cellular and molecular pathology in Tourette syndrome. In: Martino D, Leckman JF, editors. *Tourette Syndrome*. New York: Oxford University Press.
- Kalanithi PS, Zheng W, Kataoka Y, DiFiglia M, Grantz H, Saper CB, *et al.* (2005): Altered parvalbumin-positive neuron distribution in basal ganglia of individuals with Tourette syndrome. *Proc Natl Acad Sci U S A* 102:13307–13312.
- Kataoka Y, Kalanithi PS, Grantz H, Schwartz ML, Saper C, Leckman JF, Vaccarino FM (2010): Decreased number of parvalbumin and cholinergic interneurons in the striatum of individuals with Tourette syndrome. *J Comp Neurol* 518:277–291.
- Langmead B, Trapnell C, Pop M, Salzberg SL (2009): Ultrafast and memory-efficient alignment of short DNA sequences to the human genome. *Genome Biol* 10:R25.
- Harrow J, Denoeud F, Frankish A, Reymond A, Chen CK, Chrast J, *et al.* (2006): GENCODE: Producing a reference annotation for ENCODE. *Genome Biol* 7(suppl 1):S41–S49.
- Li H, Handsaker B, Wysoker A, Fennell T, Ruan J, Homer N, *et al.* (2009): The Sequence Alignment/Map format and SAMtools. *Bioinformatics* 25:2078–2079.
- Quinlan AR, Hall IM (2010): BEDTools: A flexible suite of utilities for comparing genomic features. *Bioinformatics* 26:841–842.
- Habegger L, Sboner A, Gianoulis TA, Rozowsky J, Agarwal A, Snyder M, Gerstein M (2011): RSEQtools: A modular framework to analyze RNA-Seq data using compact, anonymized data summaries. *Bioinformatics* 27:281–283.
- Robinson MD, McCarthy DJ, Smyth GK (2010): edgeR: A bioconductor package for differential expression analysis of digital gene expression data. *Bioinformatics* 26:139–140.
- Langfelder P, Horvath S (2008): WGCNA: An R package for weighted correlation network analysis. *BMC Bioinformatics* 9:559.
- Subramanian A, Kuehn H, Gould J, Tamayo P, Mesirov JP (2007): GSEA-P: A desktop application for Gene Set Enrichment Analysis. *Bioinformatics* 23:3251–3253.
- Kamburov A, Wierling C, Lehrach H, Herwig R (2009): Consensus-PathDB—a database for integrating human functional interaction networks. *Nucleic Acids Res* 37:D623–D628.
- Anders S, Huber W (2010): Differential expression analysis for sequence count data. *Genome Biol* 11:R106.
- Vandesompele J, De Preter K, Pattyn F, Poppe B, Van Roy N, De Paeppe A, Speleman F (2002): Accurate normalization of real-time quantitative RT-PCR data by geometric averaging of multiple internal control genes. *Genome Biol* 3 RESEARCH0034.
- Wang Q, Ishikawa T, Michiue T, Zhu BL, Guan DW, Maeda H (2012): Stability of endogenous reference genes in postmortem human brains for normalization of quantitative real-time PCR data: Comprehensive evaluation using geNorm, NormFinder, and BestKeeper. *Int J Legal Med* 126:943–952.
- Albin RL, Young AB, Penney JB (1995): The functional anatomy of basal ganglia disorders. *Trends Neurosci* 18:63–64.
- Holt DJ, Graybiel AM, Saper CB (1997): Neurochemical architecture of the human striatum. *J Comp Neurol* 384:1–25.
- Kawaguchi Y, Aosaki T, Kubota Y (1997): Cholinergic and GABAergic interneurons in the striatum. *Nihon Shinkei Seishin Yakurigaku Zasshi* 17:87–90.
- Figueredo-Cardenas G, Morello M, Sancesario G, Bernardi G, Reiner A (1996): Colocalization of somatostatin, neuropeptide Y, neuronal nitric oxide synthase and NADPH-diaphorase in striatal interneurons in rats. *Brain Res* 735:317–324.
- Zhao Y, Marin O, Hermesz E, Powell A, Flames N, Palkovits M, *et al.* (2003): The LIM-homeobox gene Lhx8 is required for the development of many cholinergic neurons in the mouse forebrain. *Proc Natl Acad Sci U S A* 100:9005–9010.
- Mori T, Yuxing Z, Takaki H, Takeuchi M, Iseki K, Hagino S, *et al.* (2004): The LIM homeobox gene, L3/Lhx8, is necessary for proper development of basal forebrain cholinergic neurons. *Eur J Neurosci* 19:3129–3141.
- Chen L, Chatterjee M, Li JY (2010): The mouse homeobox gene Gbx2 is required for the development of cholinergic interneurons in the striatum. *J Neurosci* 30:14824–14834.
- Du J, Zhang L, Weiser M, Rudy B, McBain CJ (1996): Developmental expression and functional characterization of the potassium-channel subunit Kv3.1b in parvalbumin-containing interneurons of the rat hippocampus. *J Neurosci* 16:506–518.
- Massengill JL, Smith MA, Son DI, O'Dowd DK (1997): Differential expression of K4-AP currents and Kv3.1 potassium channel transcripts in cortical neurons that develop distinct firing phenotypes. *J Neurosci* 17:3136–3147.
- Chow A, Erisir A, Farb C, Nadal MS, Ozaita A, Lau D, *et al.* (1999): K(+) channel expression distinguishes subpopulations of parvalbumin- and somatostatin-containing neocortical interneurons. *J Neurosci* 19:9332–9345.
- Goldberg EM, Watanabe S, Chang SY, Joho RH, Huang ZJ, Leonard CS, Rudy B (2005): Specific functions of synaptically localized potassium channels in synaptic transmission at the neocortical GABAergic fast-spiking cell synapse. *J Neurosci* 25:5230–5235.
- Leckman JF, Katsovich L, Kawikova I, Lin H, Zhang H, Kronig H, *et al.* (2005): Increased serum levels of interleukin-12 and tumor necrosis factor-alpha in Tourette's syndrome. *Biol Psychiatry* 57:667–673.

44. Pulido R, Cebrián M, Acevedo A, de Landázuri MO, Sánchez-Madrid F (1988): Comparative biochemical and tissue distribution study of four distinct CD45 antigen specificities. *J Immunol* 140:3851–3857.
45. Lit L, Gilbert DL, Walker W, Sharp FR (2007): A subgroup of Tourette's patients overexpress specific natural killer cell genes in blood: A preliminary report. *Am J Med Genet B Neuropsychiatr Genet* 144B: 958–963.
46. Tian Y, Gunther JR, Liao IH, Liu D, Ander BP, Stamova BS, *et al.* (2011): GABA- and acetylcholine-related gene expression in blood correlate with tic severity and microarray evidence for alternative splicing in Tourette syndrome: A pilot study. *Brain Res* 1381:228–236.
47. Tian Y, Liao IH, Zhan X, Gunther JR, Ander BP, Liu D, *et al.* (2011): Exon expression and alternatively spliced genes in Tourette Syndrome. *Am J Med Genet B Neuropsychiatr Genet* 156B:72–78.
48. Hong JJ, Loiselle CR, Yoon DY, Lee O, Becker KG, Singer HS (2004): Microarray analysis in Tourette syndrome postmortem putamen. *J Neurol Sci* 225:57–64.
49. Tian Y, Apperson ML, Ander BP, Liu D, Stomova BS, Jickling GC, *et al.* (2011): Differences in exon expression and alternatively spliced genes in blood of multiple sclerosis compared to healthy control subjects. *J Neuroimmunol* 230:124–129.
50. Fernandez TV, Sanders SJ, Yurkiewicz IR, Ercan-Sencicek AG, Kim YS, Fishman DO, *et al.* (2012): Rare copy number variants in tourette syndrome disrupt genes in histaminergic pathways and overlap with autism. *Biol Psychiatry* 71:392–402.
51. Akula N, Barb J, Jiang X, Wendland JR, Choi KH, Sen SK, *et al.* (2014): RNA-sequencing of the brain transcriptome implicates dysregulation of neuroplasticity, circadian rhythms and GTPase binding in bipolar disorder [published online ahead of print January 7]. *Mol Psychiatry*. doi:10.1038/mp.2013.170.
52. Fillman SG, Cloonan N, Catts VS, Miller LC, Wong J, McCrossin T, *et al.* (2013): Increased inflammatory markers identified in the dorsolateral prefrontal cortex of individuals with schizophrenia. *Mol Psychiatry* 18: 206–214.
53. Lerch JK, Kuo F, Motti D, Morris R, Bixby JL, Lemmon VP (2012): Isoform diversity and regulation in peripheral and central neurons revealed through RNA-Seq. *PLoS One* 7:e30417.
54. Zhou Z, Yuan Q, Mash DC, Goldman D (2011): Substance-specific and shared transcription and epigenetic changes in the human hippocampus chronically exposed to cocaine and alcohol. *Proc Natl Acad Sci U S A* 108:6626–6631.
55. Phelps PE, Houser CR, Vaughn JE (1985): Immunocytochemical localization of choline acetyltransferase within the rat neostriatum: A correlated light and electron microscopic study of cholinergic neurons and synapses. *J Comp Neurol* 238:286–307.
56. Bernacer J, Prensa L, Gimenez-Amaya JM (2012): Distribution of GABAergic interneurons and dopaminergic cells in the functional territories of the human striatum. *PLoS One* 7:e30504.
57. Gittis AH, Nelson AB, Thwin MT, Palop JJ, Kreitzer AC (2010): Distinct roles of GABAergic interneurons in the regulation of striatal output pathways. *J Neurosci* 30:2223–2234.
58. Gittis AH, Leventhal DK, Fensterheim BA, Pettibone JR, Berke JD, Kreitzer AC (2011): Selective inhibition of striatal fast-spiking interneurons causes dyskinesias. *J Neurosci* 31:15727–15731.
59. Morshed SA, Parveen S, Leckman JF, Mercadante MT, Bittencourt Kiss MH, Miguel EC, *et al.* (2001): Antibodies against neural, nuclear, cytoskeletal, and streptococcal epitopes in children and adults with Tourette's syndrome, Sydenham's chorea, and autoimmune disorders. *Biol Psychiatry* 50:566–577.
60. Murphy TK, Storch EA, Turner A, Reid JM, Tan J, Lewin AB (2010): Maternal history of autoimmune disease in children presenting with tics and/or obsessive-compulsive disorder. *J Neuroimmunol* 229: 243–247.
61. Kawikova I, Leckman JF, Kronig H, Katsovich L, Bessen DE, Ghebremichael M, Bothwell AL (2007): Decreased numbers of regulatory T cells suggest impaired immune tolerance in children with tourette syndrome: A preliminary study. *Biol Psychiatry* 61:273–278.
62. Bos-Veneman NG, Olieman R, Tobiasova Z, Hoekstra PJ, Katsovich L, Bothwell AL, *et al.* (2011): Altered immunoglobulin profiles in children with Tourette syndrome. *Brain Behav Immun* 25:532–538.
63. Swedo SE, Leonard HL, Mittleman BB, Allen AJ, Rapoport JL, Dow SP, *et al.* (1997): Identification of children with pediatric autoimmune neuropsychiatric disorders associated with streptococcal infections by a marker associated with rheumatic fever. *Am J Psychiatry* 154: 110–112.
64. Leonard HL, Swedo SE, Garvey M, Beer D, Perlmutter S, Lougee L, *et al.* (1999): Postinfectious and other forms of obsessive-compulsive disorder. *Child Adolesc Psychiatr Clin N Am* 8:497–511.
65. Brilot F, Merheb V, Ding A, Murphy T, Dale RC (2011): Antibody binding to neuronal surface in Sydenham chorea, but not in PANDAS or Tourette syndrome. *Neurology* 76:1508–1513.
66. Leckman JF, King RA, Gilbert DL, Coffey BJ, Singer HS, Dure LS 4th, *et al.* (2011): Streptococcal upper respiratory tract infections and exacerbations of tic and obsessive-compulsive symptoms: A prospective longitudinal study. *J Am Acad Child Adolesc Psychiatry* 50:108–118.
67. Swedo SE, Baird G, Cook EH Jr, Happe FG, Harris JC, Kaufmann WE, *et al.* (2012): Commentary from the DSM-5 Workgroup on Neurodevelopmental Disorders. *J Am Acad Child Adolesc Psychiatry* 51: 347–349.
68. Swedo SE, Leckman JF, Rose NR (2012): From research subgroup to clinical syndrome: Modifying the PANDAS criteria to describe PANS (Pediatric Acute-onset Neuropsychiatric Syndrome). *Pediatr Ther* 2:1–8.
69. Schafer DP, Lehrman EK, Kautzman AG, Koyama R, Mardinly AR, Yamasaki R, *et al.* (2012): Microglia sculpt postnatal neural circuits in an activity and complement-dependent manner. *Neuron* 74:691–705.